Cerebral Cortex, June 2018;28: 2059–2070

doi: 10.1093/cercor/bhx111
Advance Access Publication Date: 11 May 2017
Original Article

ORIGINAL ARTICLE

Spatial Asymmetry and Short-Term Suppression Underlie Direction Selectivity of Synaptic Excitation in the Mouse Visual Cortex

Ya-tang Li[1,2,3], Qi Fang[1,3], Li I. Zhang[1,2] and Huizhong Whit Tao[1,4]

[1]Zilkha Neurogenetic Institute, Keck School of Medicine, University of Southern California, Los Angeles, CA 90089, USA, [2]Department of Physiology and Biophysics, Keck School of Medicine, University of Southern California, Los Angeles, CA 90089, USA, [3]Graduate Program in Neuroscience, Keck School of Medicine, University of Southern California, Los Angeles, CA 90089, USA and [4]Department of Cell and Neurobiolog, Keck School of Medicine, University of Southern California, Los Angeles, CA 90089, USA

Address correspondence to Huizhong Whit Tao. Email: htao@usc.edu

Abstract

Direction selectivity (DS) of neuronal responses is fundamental for motion detection. With in vivo whole-cell voltage-clamp recordings from layer (L)4 neurons in the mouse visual cortex, we observed a strong correlation between DS and spatial asymmetry in the distribution of excitatory input strengths. This raises an interesting possibility that the latter may contribute to DS. The preferred direction of excitatory input was found from the stronger to weaker side of its spatial receptive field. A simple linear summation of asymmetrically distributed excitatory responses to stationary flash stimuli however failed to predict the correct directionality: it at best resulted in weak DS with preferred direction opposite to what was observed experimentally. Further studies with sequential 2 flash-bar stimulation revealed a short-term suppression of excitatory input evoked by the late bar. More importantly, the level of the suppression positively correlated with the relative amplitude of the early-bar response. Implementing this amplitude-dependent suppressive interaction can successfully predict DS of excitatory input. Our results suggest that via nonlinear temporal interactions, the spatial asymmetry can be transformed into differential temporal integration of inputs under opposite directional movements. This mechanism may contribute to the DS of excitatory inputs to L4 neurons.

Key words: direction selectivity, in vivo whole-cell voltage-clamp recording, primary visual cortex, receptive field, synaptic input.

Introduction

Motion detection is based upon direction selectivity (DS) of individual neuron responses (Hubel and Wiesel 1962). In previous research, 2 prominent models have been proposed for the generation of DS. In the first model, excitation and inhibition are spatially displaced in the visual receptive field (RF), and inhibition is temporally delayed relative to excitation. While a stimulus moving in the preferred direction evokes an excitatory response before entering the inhibitory region, a stimulus moving in the null direction activates the inhibitory region first, resulting in inhibition which temporally overlaps and suppresses the excitatory response (Barlow and Levick 1965; Torre and Poggio 1978; Hesam Shariati and Freeman 2012; Vaney et al. 2012). In the second model, the latency of excitatory input shifts systematically across the RF. A stimulus moving in the preferred direction successively activates inputs with progressively shorter latencies, and elicits a larger summed excitatory response than a stimulus moving in the null direction (Movshon et al. 1978;

Adelson and Bergen 1985; Reid et al. 1987, 1991; McLean and Palmer 1989; Albrecht and Geisler 1991; DeAngelis et al. 1993; Emerson 1997; Livingstone 1998; Priebe and Ferster 2005, 2012). Thus, the spatial shift of temporal latencies confers direction tuning of excitatory input per se.

Previously, neurons in the dorsal lateral geniculate nucleus (dLGN) of thalamus have long been thought to be unselective for direction, and DS is thought to emerge in the thalamorecipient layer (layer 4) of primary visual cortex (V1) (Priebe and Ferster 2012). In the mouse, only recently it was reported that in fact some dLGN neurons are tuned for direction (Marshel et al. 2012; Piscopo et al. 2013; Zhao et al. 2013; Scholl et al. 2013a). However, it is unlikely that DS in layer (L)4 of the cortex can be attributed to a simple relay of LGN DS, as suggested by several lines of evidence. First, only a small fraction of dLGN neurons are direction selective (Piscopo et al. 2013; Zhao et al. 2013). Second, these direction-selective dLGN neurons are mostly located in the shell region (Piscopo et al. 2013; Cruz-Martin et al. 2014), the part of the dLGN that projects preferentially to L1 of V1, whereas the core region provides the major input to L4 (Cruz-Martin et al. 2014). This suggests that the retino-geniculo-cortical pathway carrying direction-tuned information is largely segregated from that carrying nondirection-tuned information (Cruz-Martin et al. 2014). Thirdly, DS cells in L4 are generally linear (Niell and Stryker 2008; Hei et al. 2014; Li et al. 2015a), whereas DS cells in the dLGN are generally nonlinear (Swadlow and Weyand 1985; Piscopo et al. 2013; Zhao et al. 2013; Hei et al. 2014). Fourthly, thalamocortical convergence in the sensory cortex is known to be large (Bruno and Sakmann 2006; Liu et al. 2007). For example, in the somatosensory cortex it has been estimated that about 80 thalamic neurons provide convergent inputs to a L4 neuron (Bruno and Sakmann 2006). Recent Ca^{2+} imaging studies further suggest that LGN inputs to L4 exhibit a broad range of direction tuning, with a majority of them being nondirection-selective (Kondo and Ohki 2016, but see Sun et al. 2016). This leaves a large room for cortical processes (including those at thalamocortical synapses) to play a role.

In the mouse L4, we previously analyzed excitatory and inhibitory synaptic responses underlying DS (Li et al. 2015a). We found that excitatory input is tuned whereas inhibition is untuned (Li et al. 2015a). Inhibition and excitation do exhibit spatial offsets to some degree: although excitatory and inhibitory RFs largely overlap, the spatial distribution of inhibitory input strengths is symmetric, while that of excitatory input strengths is skewed. This leads to differential temporal interactions between excitation and inhibition under stimuli of opposite directions, resulting in inhibitory sharpening of DS inherent in excitatory input (Li et al. 2015a). The mechanism for the direction tuning of excitatory input itself, however, has not been addressed. We observed a correlation between DS and spatial asymmetry (skewness) of excitatory input strengths, but how the latter may contribute to the direction tuning remains unclear. In this study, using in vivo whole-cell recording and neural simulation, we discovered that a short-term suppressive interaction between sequentially activated excitatory inputs within an asymmetrically distributed RF can confer DS of excitation consistent with the experimental observation.

Materials and Methods

Animal Preparation

All experimental procedures used in this study were approved by the Animal Care and Use Committee of USC. Female adult mice (9–12 weeks, *C57BL/6*) were sedated with an intramuscular injection of chlorprothixene (10 mg/kg in 4 mg/mL water solution) and then anesthetized with urethane (1.2 g/kg, i.p., at 20% (w/v) in saline). Lactated Ringer's solution was administrated at 3 mL/kg/h to prevent dehydration. The animal's body temperature was maintained at ~37.5° by a heating pad (Harvard Apparatus). A tracheotomy was performed, and a small glass capillary tube was inserted to maintain a free airway. Cerebrospinal fluid draining was performed. The part of the skull and dura mater (~1 × 1 mm) over the V1 was removed. An artificial cerebrospinal fluid solution (ACSF, containing in mM: 140 NaCl, 2.5 KCl, 2.5 $CaCl_2$, 1.3 $MgSO_4$, 1.0 NaH_2PO4, 20 HEPES, 11 glucose, pH 7.4) was applied onto the exposed cortical surface when necessary. The eyes were covered with ophthalmic lubricant ointment until recording, at which time the eyes were rinsed with saline and a thin layer of silicone oil (30 000 cSt) was applied to prevent drying while allowing clear optical transmission. The eye positions were stable in anesthetized mice and RF drifts were negligible within the recording time windows (Mangini and Pearlman 1980; Niell and Stryker 2008; Liu et al. 2010).

In Vivo Electrophysiology

Whole-cell recordings were performed with an Axopatch 200B (Molecular Devices) according to previous studies (Moore and Nelson 1998; Zhang et al. 2003; Li et al. 2010, 2013a, 2013b). The patch pipette had a tip opening of ~2 μm (4–5 MΩ). With such large pipette openings, our blind whole-cell recordings almost exclusively sampled from excitatory neurons (Liu et al. 2010). For voltage-clamp recordings, the Cs^+-based intrapipette solution contained (in mM): 125 Cs-gluconate, 5 TEA-Cl, 4 MgATP, 0.3 GTP, 8 phosphocreatine, 10 HEPES, 10 EGTA, 2 CsCl, 1 QX-314, 0.75 MK-801, pH 7.25. For current-clamp recordings, the K^+-based intrapipette solution contained (in mM): 130 K-gluconate, 2 KCl, 1 $CaCl_2$, 4 MgATP, 0.3 GTP, 8 phosphocreatine, 10 HEPES, 11 EGTA, pH 7.25. The pipette capacitance and whole-cell capacitance were compensated completely, and series resistance was compensated by 40–50% (100 μs lag) to achieve 10–15 MΩ effective series resistance. An 11 mV junction potential was corrected. Signals were filtered at 2 kHz for voltage-clamp recording and 5 kHz for current-clamp recording and sampled at 10 kHz. The evoked excitatory currents were recorded by clamping the cell at –70 mV. For cell-attached loose-patch recordings, glass electrodes containing ACSF were used. Instead of a giga-ohm seal, a 100–250 MΩ seal was formed on the targeted neuron. The pipette capacitance was completely compensated. The spike signal was filtered at 10 kHz and sampled at 20 kHz. All neurons recorded in this study were located at a depth of 375–500 μm below the pia according to the microdrive reading, corresponding to L4 (Ma et al. 2013; Li et al. 2012, 2013b, 2015a).

Visual Stimulation

Stimuli were created using Matlab with Psychophysics Toolbox and displayed with a gamma-corrected LCD monitor (refresh rate 75 Hz) placed 0.25 m away from the right eye. The center of the monitor was placed at 45° Azimuth, 25° Elevation, and it covered ±35° horizontally and ±27° vertically of the mouse visual field. Recordings were made in the monocular zone of the V1. Spontaneous activity was recorded when a uniform gray background (luminance: 41.1 cd/m^2) was applied. In our previous study (Li et al. 2015a), we showed that L4 excitatory neurons in the mouse V1 often exhibit much stronger spike responses to flash stimuli of one sign of contrast (On or Off)

than the other, and thus these cells can be more appropriately classified as S1 cells (simple cells with only one subfield). In addition, all cells exhibit the same preferred direction under bright and dark bar stimulation. Based on these previous results, in this study, to measure DS and the underlying RF, we used moving bars and flash bars of the cell's preferred contrast. That is, if the cell preferred On stimuli, we used bright moving bars to measure DS and bright flash bars to measure RF, and vice versa. The On/Off RF of the cell was first roughly mapped with a set (6 × 8) of flash bright (57.5 cd/m^2) and dark (24.7 cd/m^2) squares (10° size) in pseudorandom sequence to determine the preferred contrast. To examine DS, drifting bars (4° width, 60° length, 50°/s speed, of preferred contrast, light or dark) of 12 directions were applied in a pseudorandom sequence for 5–10 repetitions. Drifting bars were used because they are a simple type of stimulation and mainly test responses to a single polarity of contrast. Bars moved across the screen with a 1.5 s rest time between 2 stimuli. As we have shown in our previous study (Li et al. 2015b), the preferred orientation of the V1 cell in terms of output responses is always the same as the preferred orientation of its excitatory input. We measured orientation tuning of excitatory input with drifting bars, and the preferred orientation was determined from the vector sum of the average responses for different testing orientations. Bars of this orientation were then used to map the 1D RF.

For sequential flashing-bar stimulation, a set of bars of preferred contrast at one of testing orientations were flashed (for 80 ms) sequentially across the visual field with zero rest time between consecutive bars, in one of testing directions. The sequence of moving direction was randomized. 1.5 s rest time was applied between 2 consecutive sets of bars. Based on our previous studies (Li et al. 2010, 2015a), 15 flashing bars with 4° bar width in most cases can cover the entire synaptic RF of V1 neurons. Because the speed of the moving bar was 50°/s, it would take the moving bar 80 ms to move 4° forward. Therefore 80 ms sequential flashing bars would approximately simulate a moving-bar stimulation. Bars with 160 ms duration and 8° bar width were used as a comparison. To map spatial RFs, bars (4° width, 60° length) of optimal orientation and contrast (bright or dark) at 15 positions were flashed (duration = 80 ms, interstimulus-interval = 500 ms) in a pseudorandom sequence (i.e., sequence was designed to avoid stimulating adjacent RF locations sequentially). Each location was stimulated 10 times. For 2-bar stimulation, bar positions were selected based on the mapped RF. The duration of single bars was 80 ms. The interval between 2 bars varied from 80 to 640 ms. Stimulation was repeated for 10 times.

Data Analysis

For spike responses, peristimulus spike time histograms (PSTHs, 200 ms bin size) were generated for each direction from all repetitions. To measure the similarity between a drifting-bar-evoked spike response and a response evoked by sequential flashing bars in the same direction, for each cell, we first selected directions that evoked responses larger than the spontaneous firing rate by 3 standard deviations of baseline fluctuations in either stimulation paradigm. For these directions, Pearson's correlation coefficient was calculated for evoked spike numbers of all bins between drifting bar and sequential flashing bars paradigms.

In current-clamp recordings with the K^+ gluconate-based intrapipette solution, spikes were removed with an 8-ms median filter (Li et al. 2012), and the residual subthreshold V_m response was analyzed. In voltage-clamp recordings, the excitatory responses traces were first smoothed by averaging within a sliding 40 ms window (Li et al. 2012), and the peak amplitude was then determined and used to plot tuning curves. The peak intracellular or spike responses across directions were fit with 2 Gaussian curves centered on φ_{pref} and φ_{pref} + 180°, of equal variances (σ^2) but different amplitudes (A_1 and A_2):

$$R(\varphi) = A_1 \times \exp\left(-\frac{(\varphi - \varphi_{pref})^2}{2\sigma^2}\right) + A_2 \times \exp\left(-\frac{(\varphi - \varphi_{pref} + \pi)^2}{2\sigma^2}\right) + B.$$

Direction preference was calculated based on the vector sum of the peak responses across directions, φ_{pref} = Angle $(\sum R(\varphi) \times e^{i\varphi})$. ANOVA test was performed to determine if at least response at one direction was significantly above others. P value <0.05 was used as a criterion, by which about 70% of all recorded neurons were included for further analysis. Gaussian fitting was performed for cells that passed this test. From this fit, we calculated a direction selectivity index as DSI = $(R_{pref} - R_{null})/(R_{pref} + R_{null})$, where $R_{pref} = A_1 + B$ and $R_{null} = A_2 + B$. The RF envelope of peak excitatory synaptic amplitudes was fitted with a skew-normal distribution function:

$$f(x) = \text{amplitude} \times \frac{2}{\omega} \times \varphi\left(\frac{x - \xi}{\omega}\right) \times \Phi\left(\alpha \times \frac{x - \xi}{\omega}\right) + \text{baseline},$$

where φ and Φ are the standard normal probability density function and its cumulative distribution function respectively. ξ determines the location, ω is the scale factor, and α is the shape factor. The skewness is given by:

$$\text{skewness} = \frac{4 - \pi}{2} \times \frac{(\delta \times \sqrt{2/\pi})^3}{(1 - 2\delta^2/\pi)^{3/2}}, \quad \text{with } \delta = \frac{\alpha}{\sqrt{1 + \alpha^2}}.$$

Positive skewness values were assigned if the spatial tuning curve was skewed toward the preferred side of cell as observed from experimental data. Otherwise, skewness values were negative. Cells with very low DS (DSI of excitatory input < 0.04) were not included in figures. For these neurons, their excitatory RFs were essentially nonskewed (skewness = 0.03 ± 0.06, n = 6).

To measure the reduction of the second-bar response in the 2-bar stimulation paradigm, we fit the "hidden" decay phase of the first-bar response in the 2-bar stimulation condition with exponential functions with parameters determined by fitting the single-bar response. We then subtracted the "residual" first-bar response amplitude from the total amplitude at the time point of the peak second-bar response in the 2-bar stimulation condition.

Simulation

We simulated the moving-bar response as the sum of responses to 15 sequential bars (4° width) evenly spaced in time, corresponding to a moving speed of 50°/s. All the individual-bar responses had the same temporal profile. They were modeled as:

$$G = G_{max} \times \left(1 - e^{-\frac{t - t_0}{\tau_1}}\right) \times e^{-\frac{t - t_0}{\tau_2}}, \quad \text{for } t > t_0.$$

The t_0 is the response onset latency. Fitting of the average response to flash bars yielded t_1 = 2.8 s and t_2 = 0.04 s. For each bar, G_{max} was determined by its location within the RF. The RF spatial tuning curve was modeled as a skew-normal distribution function. The latency t_0 was negatively linearly correlated with the response amplitude, with the shortest latency = 50 ms and longest latency = 100 ms.

To apply the forward suppression, each bar response was suppressed by the preceding-bar response. The relative reduction of that bar response R is given by:

$$R = 1 - e^{-kA_{i-1}},$$

where A_{i-1} is the relative amplitude of the preceding-bar response when tested individually. R equals 0 (no suppression) when A_{i-1} is 0 and approaches to 1 (complete suppression) when A_{i-1} approaches ∞. Fitting of experimental data yielded $k = 1.55$, and the value was used in the simulation. Individual-bar responses were progressively shifted by Δt (= bar width/speed), and then were summed up to give rise to the net response to a moving bar.

Results

Simulation of Moving Stimuli With Sequentially Flashed Stimuli

Previously using moving-bar stimulation, we found that about half of L4 neurons in mouse V1 are direction selective (Li et al. 2015a). In order to better understand the relationship between DS and spatial RF, it is necessary to determine the optimal parameters for stationary stimuli to be used for mapping the RF. Using in vivo cell-attached loose-patch recording, we compared the spike responses of L4 neurons to smoothly moving bars (50°/s) and sequentially flashed bars along a directional axis. The latter covered the same area within the same amount of time as the smoothly moving bar in the same direction (see Materials and Methods). We tested 2 flash durations, 80 and 160 ms. As shown by an example neuron (Fig. 1A), the cell exhibited direction-selective responses under moving-bar stimulation. Under stimulation with sequentially flashed bars of 80 ms duration, the same cell exhibited similar responses in terms of preferred direction and degree of DS. In 16 recorded L4 cells, sequentially flashed 80-ms bars evoked spike responses with their patterns having a high similarity with those of moving-bar responses, as demonstrated by the correlation coefficients close to 1 (Fig. 1B). There was no significant difference in the degree of DS, as measured with a DSI, between responses evoked by moving bars and the sequentially flashed bars (Fig. 1C). The direction along which sequentially flashed bars generated the maximum response matched the preferred direction of responses under moving-bar stimulation (Fig. 1D), and the firing rates evoked by these 2 stimulation paradigms resembled each other (Fig. 1E). In comparison, sequential flashing bars of 160-ms duration evoked responses less similar to moving-bar responses (Fig. 1B), with a significantly lower DSI (Fig. 1C). These data demonstrate that the smooth moving bar applied for stimulation in our experiments can be well simulated by sequentially flashing individual bars as brief as 80 ms.

Spatial Asymmetry, Temporal Asymmetry and DS

To further elucidate the relationship between DS and spatial RF, we recorded intracellular responses to moving bars, as well as to bars of the preferred orientation (80 ms duration) flashed

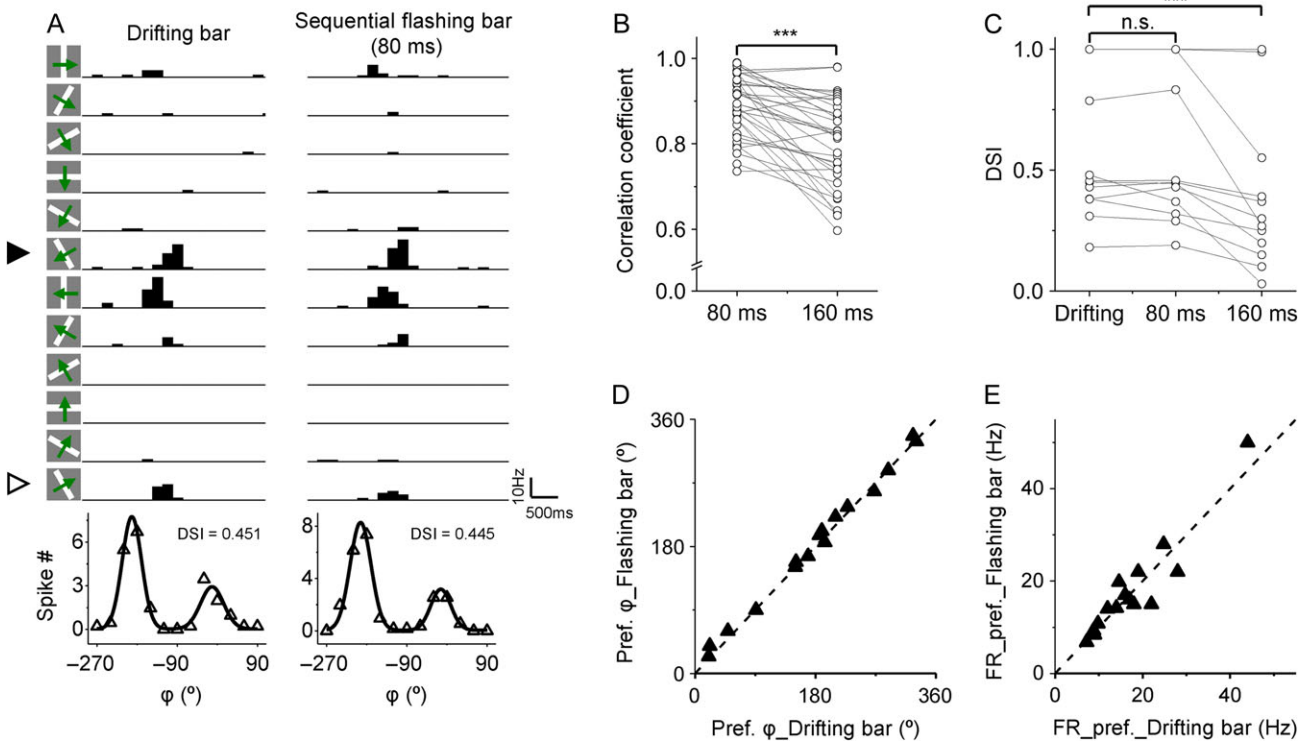

Figure 1. A drifting bar can be simulated by sequentially flashing bars along the same directional axis. (*A*) Peristimulus spike time histograms (PSTHs) for spike responses of an example L4 neuron to drifting bars of different directions (left), as well as to sequentially flashed bars (80 ms duration) in different directions (right). The direction was indicated by schematic drawings on the left, with solid and open arrowheads indicating preferred and null directions, respectively. Bottom, orientation tuning curve of evoked spike number. The DSI for each stimulation paradigm was indicated. (*B*) Average correlation coefficient calculated for responses evoked by drifting bars and sequentially flashed bars (80 or 160 ms duration) in the same neuron. Data points from the same cell are connected with a line. ***$P < 0.001$, paired *t*-test. (*C*) Comparison of DSIs calculated for responses to drifting bars and sequentially flashed bars of 80 and 160 ms duration. Data points for the same cell are connected with lines. ***$P < 0.001$, one-way ANOVA with post hoc test. (*D*) Plot of preferred direction under sequential flashing-bar (80 ms) stimulation against that under moving-bar stimulation ($n = 16$ cells). (*E*) Plot of evoked firing rate (at the preferred direction) under sequential flashing-bar (80 ms) stimulation against that under moving-bar stimulation.

randomly at different spatial locations (see Materials and Methods). We first examined membrane depolarization (V_m) responses with whole-cell current-clamp recording. As shown by an example cell in Figure 2A, the cell was tuned for direction, as manifested by a larger peak depolarization evoked by the moving bar of preferred than null direction. We also noticed a temporal difference between the preferred and null responses: it took a shorter time for the depolarization to reach the peak (i.e., time-to-peak, T_p, was faster) at the preferred than null direction (Fig. 2A, top). This suggests a potential asymmetry in the spatial distribution of synaptic inputs. Interestingly, the ratio of T_p between preferred and null responses negatively correlated with that of response amplitude (Fig. 2B), with the latter reflecting the level of direction tuning. Indeed, by quantifying DSI, we found a negative correlation between the ratio of Tp and DS (Fig. 2C), suggesting that DS might be related to spatial asymmetry.

In the same cell, we then mapped 1D RF of V_m responses with 15 flashing bars of the cell's preferred contrast (see Materials and Methods). The cell exhibited depolarizing V_m responses at multiple locations without signs of hyperpolarizing responses (Fig. 2A, bottom panel). It is somewhat different from cat simple cells in that spatially segregated depolarizing and hyperpolarizing responses are observed within their RF (Hirsch et al. 1998). However, this result is consistent with several previous studies showing a large spatial and temporal overlap of excitation and inhibition in mouse simple cells (Liu et al. 2010, 2011; Scholl et al. 2013b). We fitted the envelop of response peaks with a skew-normal function (Fig. 2A, bottom panel). The spatial RF was clearly asymmetric, with a skewness value of 0.72. In addition, the preferred direction of the cell, which was determined based on the moving-bar responses (in Fig. 2A, top panel), pointed from the stronger side to weaker side (i.e., from the short-tail to long-tail side) of the RF (Fig. 2A, bottom panel, blue arrow). In other words, the RF was skewed towards the preferred side of the cell. We quantified RF skewness for 9 similarly recorded cells. All the cells exhibited positive skewness values (Fig. 2D, see Materials and Methods), indicating that an asymmetric RF was always skewed towards the preferred side of the cell. The ratio of T_p strongly correlated with RF skewness (Fig. 2D), which also correlated with DSI (Fig. 2E). These data suggest that the temporal asymmetry of moving-bar responses, the spatial asymmetry of flashing-bar responses, and DS are closely interrelated. The more skewed the RF, the more direction selective is the neuron.

We next directly examined excitatory synaptic inputs by clamping the cell's membrane potential at −70 mV in voltage-clamp recording. We observed similar temporal and spatial asymmetry in excitatory inputs (Fig. 2F) as in membrane potential responses. In a group of 16 cells from voltage-clamp recordings, strong correlations were found between the ratio of T_p, skewness of RF and DSI of excitatory input (Fig. 2G–J). The correlation between RF skewness and DSI was consistent with our previous observation (Li et al. 2015a). These results indicate that the interrelationship between the spatial asymmetry, temporal asymmetry and DS is inherent in excitatory input. This interrelationship can be illustrated as such: neurons exhibiting a strongly asymmetric excitatory input RF also exhibit strong DS in their excitatory responses to moving bars, and the preferred direction is always against the direction towards which their RF is skewed (Fig. 2K). In our recorded population, there were both cells tested with bright bars and those tested with dark bars. Thus, our conclusion holds both for cells preferring bright and those preferring dark stimuli.

Linear Summation Fails to Predict Correct Directionality

To examine whether the spatial asymmetry of excitatory input RF per se can cause DS, we intended to predict DS by linearly summating excitatory inputs evoked by individual flash bars. As shown in Figure 3A, we simulated a set of flash-bar responses by fitting the experimentally obtained average response trace with a mathematical function (see Materials and Methods). For simplicity, they had a similar temporal profile, and the peak amplitude of each of them was assigned based on the location of the corresponding bar within the spatial RF with the latter exhibiting a skew-normal profile (Fig. 3A, red curve). We first assumed that they all had the same onset latency. Based on our experimental results that sequentially flashing bars is equivalent to presenting a drifting bar for the measurement of DS (Fig. 1), we predicted DS by simulating sequentially flashing bars using the same parameters as in the experiment. Each flash-bar response was shifted by a temporal delay based on when the corresponding location would be stimulated, and all the individual-bar responses were then summed together. As shown in Figure 3B, bars sweeping in opposite directions produced summed responses of different temporal profiles, with different delays to reach the response peak, consistent with the experimental observations. However, not much DS was produced in terms of peak response amplitude. The response to the null direction was even slightly larger than that to the preferred direction (Fig. 3B). We next varied the skewness level of the spatial RF, and quantified the degree of DS for the simulated responses (Fig. 3C). For a symmetric RF, no DS was generated (i.e., DSI ~0). When the skewness level was increased, at best very weak DS was produced. However, the predicted preferred direction was opposite to what would be expected based on our experimental observations, as demonstrated by the negative values of DSI (Fig. 3C).

In the previous excitatory model for DS, a progressive change in the onset latency of excitatory inputs across the RF results in differential summation under opposite directional movements. We thus examined the onset latencies of flash-bar-evoked excitatory responses. As shown by the intensity-coded time-dependent amplitude for bars at different locations (Fig. 3D), the strongest response (i.e., response at the RF peak) had the shortest onset latency, while responses at RF edges had longer onset latencies, forming a V-shape profile of latency distribution across the RF (Fig. 3D). Across the cells examined, the onset latency exhibited a negative correlation with the peak response amplitude (Fig. 3E). However, even when we introduced this amplitude-dependent change in onset latency into our simulated responses (Fig. 3E, inset), the predicted preferred direction was still opposite to what was observed experimentally (Fig. 3F, red). Together, these simulation results demonstrate that a simple linear summation of flash-bar responses across the RF does not account for the relationship between RF skewness and direction tuning. This suggests that some nonlinear mechanism might be involved.

Amplitude-Dependent Short-Term Suppression

To test potential nonlinear interactions, we employed a sequential-bar stimulation paradigm. Two adjacent bars within the excitatory input RF were flashed individually, or sequentially (bar 1 followed by bar 2) with different interbar intervals (Fig. 4A). We compared the amplitudes of the second-bar-evoked excitatory responses, when bar 2 was

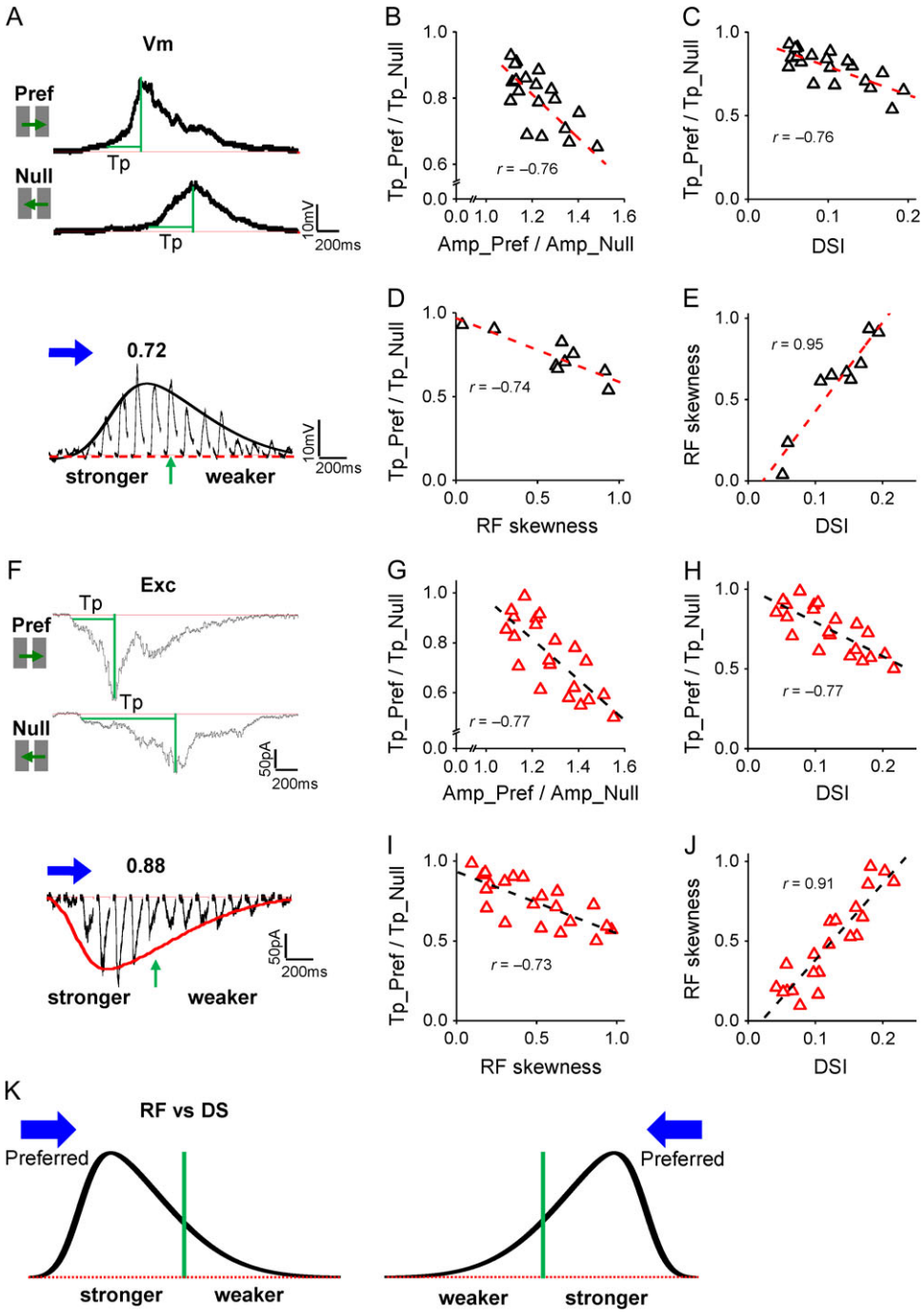

Figure 2. A strong correlation between DS and RF asymmetry. (*A*) Top panel, membrane potential (V_m) responses (average form 5 trials) of an example L4 cell to bright drifting bars of preferred and null directions. Red dash line marks the level of resting membrane potential. Vertical green line labels the response peak. Horizontal green line labels the time from 10% peak to peak (i.e., T_p). Bottom panel, V_m responses (average from 10 trials) of the same cell evoked by bright flashing bars (4° width) at different locations, presented in a pseudorandom sequence. The envelope for the peak response amplitudes was fit with a skew-normal distribution function (solid curve). The skewness value is 0.72. Blue arrow marks the cell's preferred direction based on responses to drifting bars. Green arrow marks the midpoint of the spatial RF. The stronger and weaker sides of the RF are marked. Note that for simplicity, all RFs are arranged so that they are skewed toward the left side in all data presentation. (*B*) Ratio of Tp between preferred and null V_m responses versus ratio between the response peak amplitudes (n = 20 cells). Red dash line is the best-fit linear regression line. The correlation coefficient (r) is indicated. P = 1e – 4. (*C*) Ratio of T_p versus DSI. P = 1e – 4. (*D*) Ratio of Tp versus RF skewness (n = 9 cells). P = 0.02. (*E*) RF skewness versus DSI. P = 9e – 5. (*F*) Top panel, excitatory synaptic responses (average form 5 trials) of an example neuron to bright drifting bars of preferred and null directions. Bottom panel, excitatory synaptic responses of the same cell evoked by bright flashing bars at different locations. Data are presented in a similar way as in (*A*). (*G*) Ratio of T_p between preferred and null excitatory responses versus ratio between the response peak amplitudes (n = 21 cells). P = 4e – 5. (*H*) Ratio of T_p between preferred and null responses versus DSI for excitatory input. P = 4e – 5. (*I*) Ratio of T_p versus RF skewness. P = 2e – 4. (*J*) RF skewness versus DSI. P = 1e – 8. (*K*) Schematic illustration of the relationship between RF asymmetry and DS. Blue arrow marks the preferred direction under drifting bar stimulation.

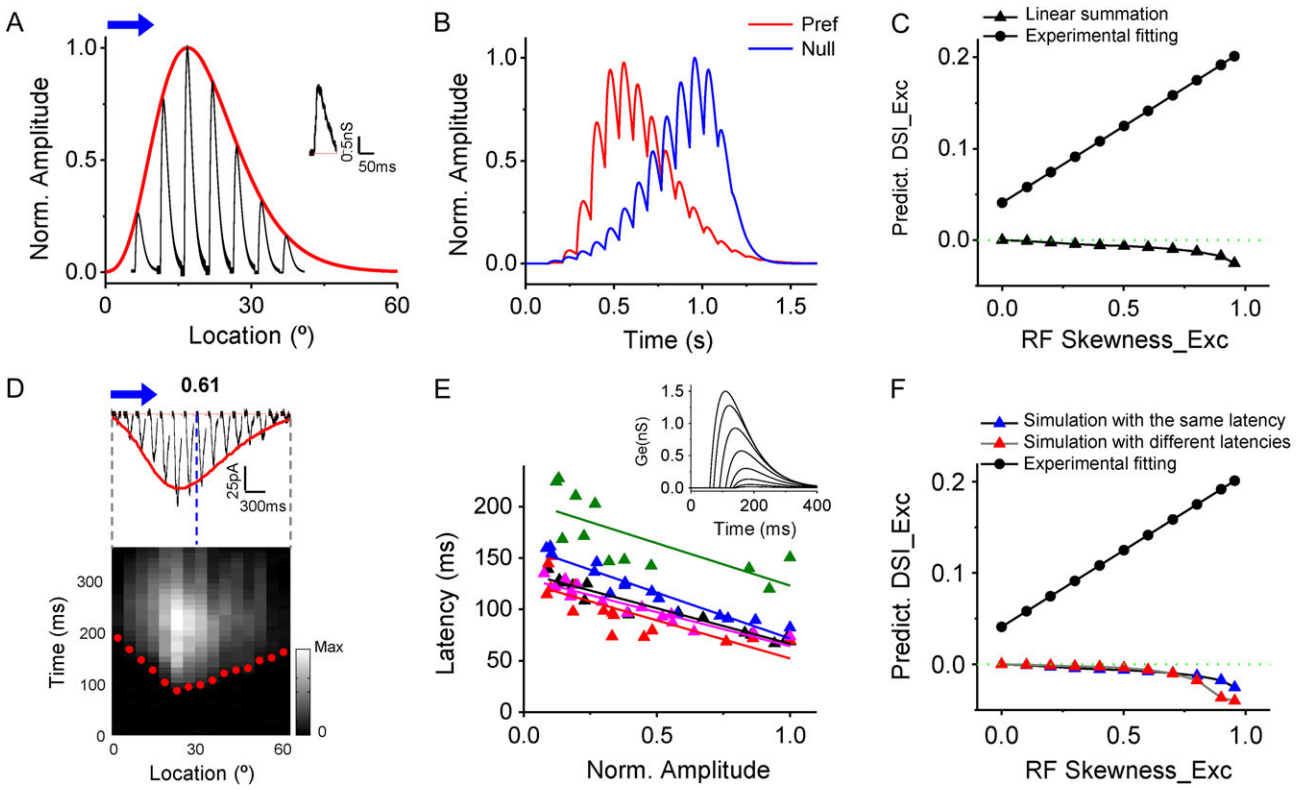

Figure 3. Simple linear summation does not predict correct directionality. (*A*) Simulated excitatory responses evoked by flashing bars at different locations within a skewed RF (red curve depicts the envelop for peak response amplitudes; skewness = 0.8). Only responses to a subset of the bars are shown due to crowdedness. All the responses have the same onset latency. Blue arrow marks the expected preferred direction according to experimental observations. Inset, average bar-evoked excitatory response from experimental data. (*B*) Summing up individual-bar responses after shifting each with an appropriate delay produced simulated responses to drifting bars of preferred and null directions (normalized). Note that the null response is slightly larger than the preferred response. (*C*) Predicted DSI of excitatory input using simple linear summation (triangle) plotted against the RF skewness. Circle represents the expected DSI based on experimental observations. Green dash line indicates zero. (*D*) Top, excitatory inputs evoked by flashing bars at different locations in an example cell. The RF skewness is 0.61. Bottom, intensity plot of time-dependent synaptic amplitude for bars at different locations. Red dots mark the onset latencies. (*E*) Onset latency versus peak response amplitude. Data points for the same cell are in the same color. Colored lines are the best-fit linear regression lines. Inset, temporal profiles of simulated flash-bar-evoked excitatory responses after considering the amplitude-dependent differential onset latencies. (*F*) Predicted DSI of excitatory input from summation of flash-bar responses with differential onset latencies (red triangle) versus RF skewness.

applied alone or preceded by bar 1. As shown by an example cell (Fig. 4*A*), compared with the single flash, bar 2 evoked response was reduced in amplitude when preceded by bar 1. This reduction was more obvious at 120 ms than 640 ms interbar interval. Across the cells tested with sequential-bar stimulation, we observed that the reduction of bar 2 response (as compared with the amplitude of the single-bar response) decreased with increasing interbar intervals, and nearly disappeared at 640 ms interbar interval (Fig. 4*B*). Thus, the suppressive interaction is only short-term. Interestingly, at the same interbar interval (80 ms), the reduction of bar 2 response positively correlated with the relative amplitude of bar 1 response (Fig. 4*C*, $r = 0.80$, $P < 0.05$). Therefore, our data suggest that the stronger the bar 1 response, the larger suppression can it exert on the following bar 2 evoked response. The relationship between the level of suppression and relative bar one response amplitude could be fit with an arithmetic function (Fig. 4*C*). Notably, there was no significant correlation between the level of suppression and the absolute amplitudes of individual-bar responses, or the maximum response amplitude under the 2-bar stimulation condition (Fig. 4*D–F*), suggesting that the suppression cannot be simply attributed to a response saturation, but rather reflects a history-dependent dynamic property.

Next, we wondered if the amplitude-dependent suppression could be observed directly within the same RF. To this end, we first examined which bar response contributed most importantly to the summed response under moving-bar stimulation. Notably, the timing of the peak moving-bar response matched relatively well with that for the moving bar to hit the RF peak (Fig. 4*G*). In other words, when a drifting bar hits the RF peak, response reaches the maximal level. Therefore, the responses evoked by bars at and just before the RF peak were probably the most important factor to contribute to the peak amplitude of the drifting-bar response. We then designed a 3-bar testing paradigm: bar 2 was located at the RF peak, with adjacent bar 1 and bar 3 on different sides of it (Fig. 4*H*). Since the RF was skewed, bar 1 and bar 3 evoked responses of different amplitudes (bar 1 < bar 3, Fig. 4*H*). We next applied sequential-bar stimulation: bar 1 followed by bar 2 (i.e., in the preferred direction), or bar 3 followed by bar 2 (i.e., in the null direction). As shown by the example cell in Figure 4*H*, bar 2 response was apparently larger in the "1-2" than "3-2" pairing condition, confirming that a weaker preceding bar had a weaker suppressive effect. A similar trend was observed in all cells tested: the response to the stimulation of RF peak was less suppressed by a preceding bar when the sequential-bar stimulation was applied in the preferred (1-2) than null (3-2) direction (Fig. 4*I*).

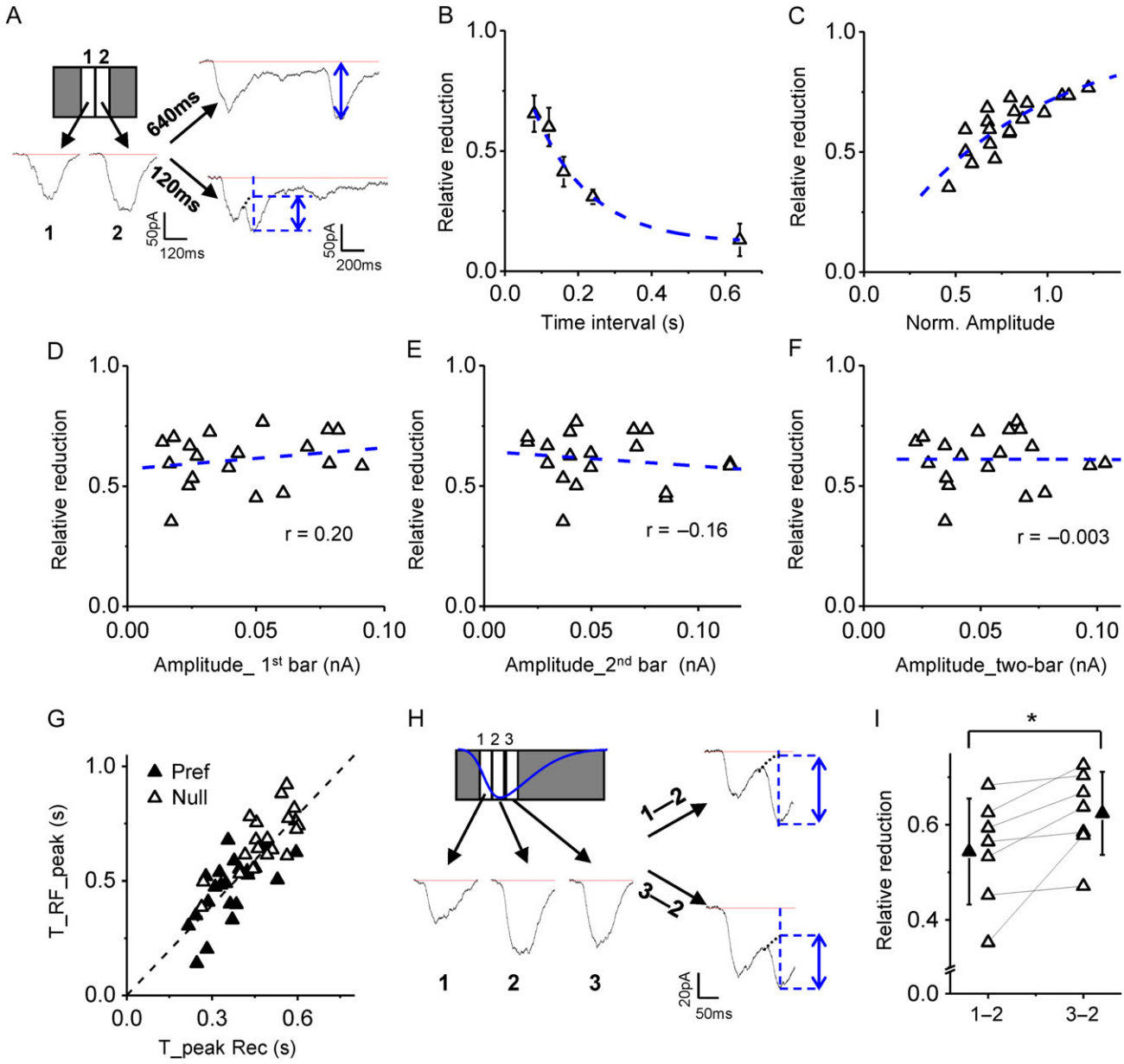

Figure 4. Amplitude-dependent suppression of excitatory input. (*A*) Average excitatory responses of an example neuron to 2 adjacent bars within its RF either flashed individually (left panel) or flashed sequentially (right panel) with 640 ms (upper) and 120 ms (lower) interbar-intervals. Dotted curve depicts the fitted decay of the first-bar response. Blue arrow marks the calculated amplitude of the second-bar response under the sequential-bar stimulation. (*B*) Relative reduction of the second-bar response versus interbar-interval. Bar = SEM; $n = 8$ cells. Dotted curve represents the fitting function: $y = 0.95^{*}\exp(-x/151) + 0.12$. (*C*) Relative reduction of the second-bar response versus normalized amplitude of the first-bar response (to the second-bar response when tested individually). Blue curve represents the fitting of the data. Function: $y = 1 - \exp(-1.24^{*}x)$. Adjusted *R*-square = 0.67. (*D*) Relative reduction of bar 2 response versus the absolute peak amplitude of the first-bar response (individually flashed). $P = 0.41$. (*E*) Relative reduction versus the absolute peak amplitude of the second-bar response (individually flashed). $P = 0.51$. (*F*) Relative reduction versus the absolute peak amplitude of the 2-bar response (sequentially flashed). $P = 0.99$. (*G*) Estimated time for a drifting bar to hit the RF peak versus the time for the recorded response to reach maximum. Solid, preferred direction; open, null direction. Dash line is the identity line. (*H*) Three-bar experiment in an example cell. The reference bar (bar 2) was chosen to be at the RF peak. Left, excitatory responses to the 3 bars applied individually. Right, responses to sequential bars of "1-then-2" and "3-then-2" sequences, respectively. The interbar-interval was 120 ms. (*I*) Relative reduction of the reference-bar response in "1-then-2" and "3-then-2" stimulation paradigms. $^{*}P < 0.05$, paired *t*-test.

Spatial Asymmetry Plus Amplitude-Dependent Suppression Correctly Predicts DS

The above data suggest that bars drifting in opposite directions would generate differential suppression effects. To test whether this could lead to differential response levels, we introduced an amplitude-dependent suppression algorithm into our simulation. Here, we assumed that as a bar drifts across the RF, activation of each bar location imposes suppression of the response to the subsequent bar location, with the suppression level determined by the amplitude of the current bar response relative to the subsequent bar response, as depicted by the fitting curve in Figure 4C. Interestingly, the introduction of such amplitude-dependent suppression did produce differential response levels for bars drifting in opposite directions, and the direction that

generated a larger response matched the preferred direction as observed experimentally (Fig. 5A). In addition, it took a shorter time for the response to reach the peak at the preferred than null direction (Fig. 5A, arrows), also consistent with our experimental observations. As the skewness level increased, stronger DS was generated (Fig. 5B, black). Applying differential onset latencies to individual-bar responses even produced a slightly better effect (Fig. 5B, gray).

Finally, we predicted direction tuning using experimentally obtained flash-bar responses. When individual-bar responses were simply linearly summated, the predicted DSI failed to match the experimentally observed DSI (Fig. 5C, open triangle, $r = -0.08$), and the prediction of preferred direction was wrong for most neurons. In contrast, when we introduced the amplitude-dependent suppression algorithm, the predicted DSI conformed to the experimentally observed DSI (Fig. 5C, filled circle, $r = 0.84$, $P < 0.05$). Together, these prediction results strongly suggest that an asymmetric distribution of excitatory input strengths together with an amplitude-dependent suppression mechanism can be sufficient for producing correct DS.

Discussion

A Proposed Model for DS Based on RF Asymmetry

The mechanisms underlying the generation of DS in the cortex have been intensively debated (Livingstone 2005; Priebe and Ferster 2012). In the past, with the understanding that dLGN neurons are mostly not direction tuned, a progressive change in the temporal delay of excitatory inputs across the RF has become a dominant model to explain how nontuned thalamic inputs are transformed into tuned cortical responses (Movshon et al. 1978; Adelson and Bergen 1985; Reid et al. 1987, 1991; McLean and Palmer 1989; Albrecht and Geisler 1991; DeAngelis et al. 1993; Emerson 1997; Livingstone 1998; Priebe and Ferster 2005). Indeed, in cat DS simple cells, a systematic shift of temporal profile of responses to flash stimuli has been observed, resulting in a "slant" in the spatial-temporal space (DeAngelis et al. 1993; Priebe and Ferster 2005). In the mouse, while some dLGN neurons do have DS, as we have reasoned in the introduction, cortical mechanisms likely contribute to DS observed in L4, although how much they contribute remains an open question (Kondo and Ohki 2016; Sun et al. 2016). Different from cat DS simple cells, we found that the onset latency of excitatory input has a negative relationship with its response amplitude, resulting in a V-shape (instead of a slant) profile in the spatial-temporal space. In fact, this is also the case for inhibitory responses to flash stimuli (Li et al. 2015a). Although this could reflect a species difference, our results on the other hand are consistent with a study in the cat which was not particularly focused on DS cells (Bringuier et al. 1999). The latter study reported that "synaptic depolarizing responses to stimuli flashed at increasing distances from the center of the RF decreased in strength, whereas their onset latency increased." As we showed in the simulation with linear summation, such V-shaped distribution of latencies alone failed to correctly predict the preferred direction as experimentally observed.

In this study, we propose a new model that spatial asymmetry of excitatory input strengths together with an amplitude-dependent suppressive interaction can be sufficient for producing correct direction tuning. As shown by the schematic illustration of a simplified asymmetric RF containing 2 subregions (Fig. 6A), the response to stimulation of the stronger subregion is differentially influenced under opposite directional movements: it is less suppressed under preferred than null directional movements, resulting in a larger summed response under the preferred directional movement (Fig. 6B,C). This model can explain well the relationship between DS and RF skewness as observed in our experiments, that is, the preferred direction is against the direction toward which the RF is skewed. In this model, differential response latencies across the RF are not required for producing direction tuning.

It should be noted that our current model is based on simulation results. While there is a strong correlation between DS and RF asymmetry, as well as between the level of suppression and relative response amplitude, a causal relationship between these observed phenomena remains to be firmly established.

Potential Mechanisms for the Amplitude-Dependent Suppression

In the proposed DS model, the amplitude-dependent suppression is critical for producing the correct directionality. However, the mechanism underlying the observed correlation between amplitude and level of suppression is unclear. Nonlinear interactions between 2 sequential stimuli in terms of spiking responses have been widely observed in visual and auditory cortices (e.g., 2-tone suppression) (Emerson et al. 1987; Brosch and Schreiner 1997; Conway and Livingstone 2003; Zhang et al. 2003). In this study, we show that sequential-stimulus suppression can

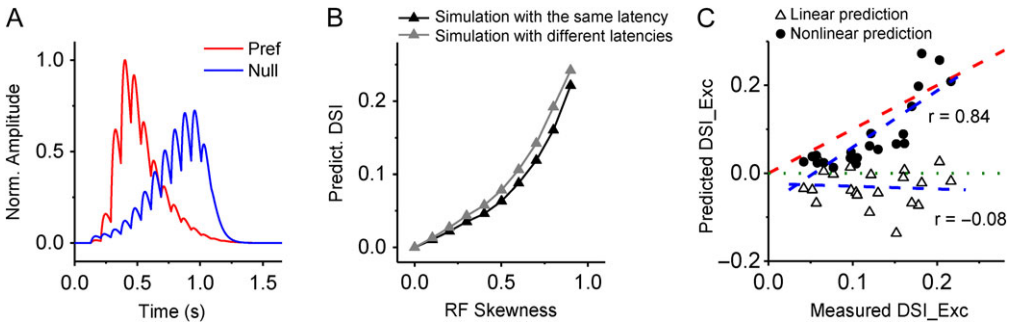

Figure 5. Asymmetric RF plus amplitude-dependent suppression correctly predicts DS. (*A*) Simulated moving-bar responses to preferred and null directions (normalized) when an amplitude-dependent suppression algorithm was incorporated. The RF skewness is 0.8, same as in Figure 3A. (*B*) Predicted DSI of excitatory responses when incorporating the amplitude-dependent suppression versus RF skewness. Black, flashing-bar responses have the same onset latency. Gray, flashing-bar responses have different onset latencies. (*C*) Predicted DSI from experimentally obtained flashing-bar responses versus measured DSI of recorded moving-bar responses. Open, simple linear summation; solid, incorporating the amplitude-dependent suppression. Red dash line is the identity line. Green dash line indicates zero. Blue dash lines are the best-fit linear regression lines. $n = 21$ cells. For linear prediction, $r = -0.08$, $P = 0.73$. For nonlinear prediction, $r = 0.84$, $P = 2e-6$.

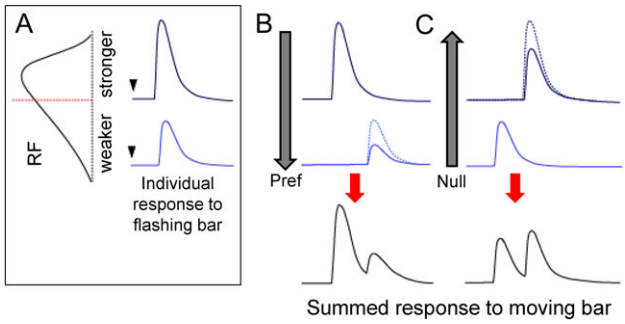

Figure 6. A proposed model for DS in L4 of the cortex. (*A*) A schematically illustrated asymmetric RF containing a stronger and a weaker subregion (left). Excitatory responses (reversed in sign) to individual stimulation of these subregions are shown on the right. Black arrowhead marks the onset of stationary (flash) stimuli. (*B*) Top, responses to stimulation of the subregions under preferred directional (PD) movements. Dash curve, original response; solid curve, response after being suppressed. Bottom, summation of all the individual responses. (*C*) Scenario under null directional (ND) movements.

occur at the level of excitatory input to cortical neurons. The reduction of the second-bar response may arise from many sources: it could be a property of the feed-forward input to the cortex, it could be due to feed-forward circuit-level inhibition of neighboring excitatory neurons that contribute to the second-bar response, or it could reflect feedback inhibition produced by the high-amplitude response to a single pulse. It is not known how much each of these potential mechanisms contribute to the observed suppression. While a suppression effect occurring at earlier stages can be relayed by feed-forward inputs to the cortex, to confer the relationship between the synaptic response amplitude as manifested in cortical cells and the level of suppressive effect it has on the subsequent response, cortical processes (including those at thalamocortical synapses) are likely involved. Two potential mechanisms may contribute to the dependency of the suppression on amplitude and interval. First, spatially adjacent bars may activate some common thalamocortical inputs, which exhibit short-term depression (Boudreau and Ferster 2005; Gabernet et al. 2005; Cruikshank et al. 2010; Kloc and Maffei 2014). Second, local cortical inhibition evoked by the first bar may reduce excitability of nearby excitatory neurons within a certain time window. Together these would reduce LGN and intracortical inputs to L4 cells in response to the second bar.

Excitatory and Inhibitory RFs

The correlation between DS and RF asymmetry also applies to inhibitory input, in that inhibitory RFs are in general symmetric and inhibitory synaptic responses are barely tuned for direction, as we previously reported for L4 neurons (Li et al. 2015a). Since excitatory RFs can be skewed while inhibitory RFs are always symmetric, excitation and inhibition may interact differentially under opposite directional movements: excitation peaks earlier than inhibition for stimuli moving in the preferred direction, whereas inhibition peaks earlier in the null direction. Such differential temporal interactions per se can lead to direction tuning of output responses (Li et al. 2015a). When excitatory input already exhibits direction tuning, symmetric inhibition is therefore able to further sharpen DS inherent in the excitatory input (Li et al. 2015a).

It is an interesting question why excitatory and inhibitory circuits exhibit different levels of RF asymmetry. Both experimental and modeling studies have shown that repeated directional stimuli can induce an asymmetric shaping of synaptic circuits through spike-timing dependent plasticity (STDP) (Mehta et al. 2000; Rao and Sejnowski 2000; Engert et al. 2002; Fu et al. 2004; Wenisch et al. 2005), suggesting that asymmetric RFs can arise through activity-dependent mechanisms. Possibly, asymmetric synaptic RFs are formed during development, under instructive influences of either wave-like endogenous activity or visually evoked activity. Some initial bias provided by the retinal input may exist to facilitate symmetry-breaking under stimuli of all different directions (Li et al. 2008), which may explain why not all excitatory cells have an asymmetric excitatory RF. In addition, the asymmetric modification by STDP only applies to excitatory connections, as plasticity of inhibitory connections as well as of excitatory connections onto inhibitory neurons is not sensitive to the temporal order of pre- and postsynaptic spiking (Bi and Poo 2001; Woodin et al. 2003; Lu et al. 2007).

Previously, we found that the thalamocortical input to L4 neurons already exhibits direction tuning, and that the thalamocortical response is just linearly amplified by intracortical circuits, preserving the level of tuning in the total excitatory input (Lien and Scanziani 2013; Li et al. 2013b). This raises a possibility that the relationship between DS and RF asymmetry may already exist at the level of thalamocortical input, which will be tested in the future.

Taken together, our results in mouse V1 revealed a relationship between asymmetric spatial distribution of excitatory input and its directional bias. Our simulation study further showed that via amplitude-dependent nonlinear interactions, the spatial asymmetry can be transformed into differential temporal integration of inputs under opposite directional movements, which may contribute to the DS of excitatory inputs to cortical neurons. Our results are reminiscent of a similar relationship between the skewness of synaptic tonal RF and DS to frequency-modulated sound sweeps in the auditory cortex (Zhang et al. 2003). This suggests that there could be a shared strategy between different cortical circuits to code temporal information in the spatial distribution of synaptic strengths.

Funding

This work was supported by grants to H.W.T. from the US National Institutes of Health (EY019049 and EY022478) and the Kirchgessner Foundation. L.I.Z. was supported by grants from the NIH (R01DC008983).

Notes

Conflict of Interest: None declared.

References

Adelson EH, Bergen JR. 1985. Spatiotemporal energy models for the perception of motion. J Opt Soc Am A. 2:284–299.

Albrecht DG, Geisler WS. 1991. Motion selectivity and the contrast-response function of simple cells in the visual cortex. Vis Neurosci. 7:531–546.

Barlow HB, Levick WR. 1965. The mechanism of directionally selective units in rabbit's retina. J Physiol. 178:477–504.

Bi G, Poo M. 2001. Synaptic modification by correlated activity: Hebb's postulate revisited. Annu Rev Neurosci. 24:139–166.

Boudreau CE, Ferster D. 2005. Short-term depression in thalamocortical synapses of cat primary visual cortex. J Neurosci. 25:7179–7190.

Bringuier V, Chavane F, Glaeser L, Fregnac Y. 1999. Horizontal propagation of visual activity in the synaptic integration field of area 17 neurons. Science. 283:695–699.

Brosch M, Schreiner CE. 1997. Time course of forward masking tuning curves in cat primary auditory cortex. J Neurophysiol. 77:923–943.

Bruno RM, Sakmann B. 2006. Cortex is driven by weak but synchronously active thalamocortical synapses. Science. 312: 1622–1627.

Conway BR, Livingstone MS. 2003. Space-time maps and two-bar interactions of different classes of direction-selective cells in macaque V-1. J Neurophysiol. 89:2726–2742.

Cruikshank SJ, Urabe H, Nurmikko AV, Connors BW. 2010. Pathway-specific feedforward circuits between thalamus and neocortex revealed by selective optical stimulation of axons. Neuron. 65:230–245.

Cruz-Martin A, El-Danaf RN, Osakada F, Sriram B, Dhande OS, Nguyen PL, Callaway EM, Ghosh A, Huberman AD. 2014. A dedicated circuit links direction-selective retinal ganglion cells to the primary visual cortex. Nature. 10.1038/nature12989.

DeAngelis GC, Ohzawa I, Freeman RD. 1993. Spatiotemporal organization of simple-cell receptive fields in the cat's striate cortex. II. Linearity of temporal and spatial summation. J Neurophysiol. 69:1118–1135.

Emerson RC. 1997. Quadrature subunits in directionally selective simple cells: spatiotemporal interactions. Vis Neurosci. 14:357–371.

Emerson RC, Citron MC, Vaughn WJ, Klein SA. 1987. Nonlinear directionally selective subunits in complex cells of cat striate cortex. J Neurophysiol. 58:33–65.

Engert F, Tao HW, Zhang LI, Poo MM. 2002. Moving visual stimuli rapidly induce direction sensitivity of developing tectal neurons. Nature. 419:470–475.

Fu YX, Shen Y, Gao H, Dan Y. 2004. Asymmetry in visual cortical circuits underlying motion-induced perceptual mislocalization. J Neurosci. 24:2165–2171.

Gabernet L, Jadhav SP, Feldman DE, Carandini M, Scanziani M. 2005. Somatosensory integration controlled by dynamic thalamocortical feed-forward inhibition. Neuron. 48:315–327.

Hei X, Stoelzel CR, Zhuang J, Bereshpolova Y, Huff JM, Alonso JM, Swadlow HA. 2014. Directional selective neurons in the awake LGN: response properties and modulation by brain state. J Neurophysiol. 112:362–373.

Hesam Shariati N, Freeman AW. 2012. A multi-stage model for fundamental functional properties in primary visual cortex. PloS One. 7:e34466.

Hirsch JA, Alonso JM, Reid RC, Martinez LM. 1998. Synaptic integration in striate cortical simple cells. J Neurosci. 18:9517–9528.

Hubel DH, Wiesel TN. 1962. Receptive fields, binocular interaction and functional architecture in the cat's visual cortex. J Physiol. 160:106–154.

Kloc M, Maffei A. 2014. Target-specific properties of thalamocortical synapses onto layer 4 of mouse primary visual cortex. J Neurosci. 34:15455–15465.

Kondo S, Ohki K. 2016. Laminar differences in the orientation selectivity of geniculate afferents in mouse primary visual cortex. Nat Neurosci. 19:316–319.

Li LY, Li YT, Zhou M, Tao HW, Zhang LI. 2013a. Intracortical multiplication of thalamocortical signals in mouse auditory cortex. Nat Neurosci. 16:1179–1181.

Li Y, Van Hooser SD, Mazurek M, White LE, Fitzpatrick D. 2008. Experience with moving visual stimuli drives the early development of cortical direction selectivity. Nature. 456: 952–956.

Li YT, Ibrahim LA, Liu BH, Zhang LI, Tao HW. 2013b. Linear transformation of thalamocortical input by intracortical excitation. Nat Neurosci. 16:1324–1330.

Li YT, Liu BH, Chou XL, Zhang LI, Tao HW. 2015a. Strengthening of direction selectivity by broadly tuned and spatiotemporally slightly offset inhibition in mouse visual cortex. Cereb Cortex. 25:2466–2477.

Li YT, Liu BH, Chou XL, Zhang LI, Tao HW. 2015b. Synaptic basis for differential orientation selectivity between complex and simple cells in mouse visual cortex. J Neurosci. 35:11081–11093.

Li YT, Ma WP, Li LY, Ibrahim LA, Wang SZ, Tao HW. 2012. Broadening of inhibitory tuning underlies contrast-dependent sharpening of orientation selectivity in mouse visual cortex. J Neurosci. 32:16466–16477.

Lien AD, Scanziani M. 2013. Tuned thalamic excitation is amplified by visual cortical circuits. Nat Neurosci. 16:1315–1323.

Liu BH, Li P, Sun YJ, Li YT, Zhang LI, Tao HW. 2010. Intervening inhibition underlies simple-cell receptive field structure in visual cortex. Nat Neurosci. 13:89–96.

Liu BH, Li YT, Ma WP, Pan CJ, Zhang LI, Tao HW. 2011. Broad inhibition sharpens orientation selectivity by expanding input dynamic range in mouse simple cells. Neuron. 71:542–554.

Liu BH, Wu GK, Arbuckle R, Tao HW, Zhang LI. 2007. Defining cortical frequency tuning with recurrent excitatory circuitry. Nat Neurosci. 10:1594–1600.

Livingstone MS. 1998. Mechanisms of direction selectivity in macaque V1. Neuron. 20:509–526.

Livingstone MS. 2005. Directional inhibition: a new slant on an old question. Neuron. 45:5–7.

Lu JT, Li CY, Zhao JP, Poo MM, Zhang XH. 2007. Spike-timing-dependent plasticity of neocortical excitatory synapses on inhibitory interneurons depends on target cell type. J Neurosci. 27:9711–9720.

Ma WP, Li YT, Tao HW. 2013. Downregulation of cortical inhibition mediates ocular dominance plasticity during the critical period. J Neurosci. 33:11276–11280.

Mangini NJ, Pearlman AL. 1980. Laminar distribution of receptive field properties in the primary visual cortex of the mouse. J Comp Neurol. 193:203–222.

Marshel JH, Kaye AP, Nauhaus I, Callaway EM. 2012. Anterior-posterior direction opponency in the superficial mouse lateral geniculate nucleus. Neuron. 76:713–720.

McLean J, Palmer LA. 1989. Contribution of linear spatiotemporal receptive field structure to velocity selectivity of simple cells in area 17 of cat. Vision Res. 29:675–679.

Mehta MR, Quirk MC, Wilson MA. 2000. Experience-dependent asymmetric shape of hippocampal receptive fields. Neuron. 25:707–715.

Moore CI, Nelson SB. 1998. Spatio-temporal subthreshold receptive fields in the vibrissa representation of rat primary somatosensory cortex. J Neurophysiol. 80:2882–2892.

Movshon JA, Thompson ID, Tolhurst DJ. 1978. Spatial and temporal contrast sensitivity of neurones in areas 17 and 18 of the cat's visual cortex. J Physiol. 283:101–120.

Niell CM, Stryker MP. 2008. Highly selective receptive fields in mouse visual cortex. J Neurosci. 28:7520–7536.

Piscopo DM, El-Danaf RN, Huberman AD, Niell CM. 2013. Diverse visual features encoded in mouse lateral geniculate nucleus. J Neurosci. 33:4642–4656.

Priebe NJ, Ferster D. 2005. Direction selectivity of excitation and inhibition in simple cells of the cat primary visual cortex. Neuron. 45:133–145.

Priebe NJ, Ferster D. 2012. Mechanisms of neuronal computation in mammalian visual cortex. Neuron. 75:194–208.

Rao RPN, Sejnowski TJ. 2000. Predictive sequence learning in recurrent neocortical circuits. In: SA S, TK L, KR M, editors. Advances in neural information processing systems. Cambridge(MA): MIT.

Reid RC, Soodak RE, Shapley RM. 1987. Linear mechanisms of directional selectivity in simple cells of cat striate cortex. Proc Natl Acad Sci USA. 84:8740–8744.

Reid RC, Soodak RE, Shapley RM. 1991. Directional selectivity and spatiotemporal structure of receptive fields of simple cells in cat striate cortex. J Neurophysiol. 66:505–529.

Scholl B, Tan AY, Corey J, Priebe NJ. 2013a. Emergence of orientation selectivity in the Mammalian visual pathway. J Neurosci. 33:10616–10624.

Scholl B, Tan AYY, Corey J, Priebe NJ. 2013b. Emergence of orientation selectivity in the mammalian visual pathway. J Neurosci. 33:10616–10624.

Sun W, Tan Z, Mensh BD, Ji N. 2016. Thalamus provides layer 4 of primary visual cortex with orientation- and direction-tuned inputs. Nat Neurosci. 19:308–315.

Swadlow HA, Weyand TG. 1985. Receptive-field and axonal properties of neurons in the dorsal lateral geniculate nucleus of awake unparalyzed rabbits. J Neurophysiol. 54: 168–183.

Torre V, Poggio T. 1978. A synaptic mechanism possibly underlying directional selectivity to motion. Proc R Soc Lond B Biol Sci. 202:409–416.

Vaney DI, Sivyer B, Taylor WR. 2012. Direction selectivity in the retina: symmetry and asymmetry in structure and function. Nat Rev Neurosci. 13:194–208.

Wenisch OG, Noll J, Hemmen JL. 2005. Spontaneously emerging direction selectivity maps in visual cortex through STDP. Biol Cybern. 93:239–247.

Woodin MA, Ganguly K, Poo MM. 2003. Coincident pre- and postsynaptic activity modifies GABAergic synapses by postsynaptic changes in Cl- transporter activity. Neuron. 39: 807–820.

Zhang LI, Tan AY, Schreiner CE, Merzenich MM. 2003. Topography and synaptic shaping of direction selectivity in primary auditory cortex. Nature. 424:201–205.

Zhao X, Chen H, Liu X, Cang J. 2013. Orientation-selective responses in the mouse lateral geniculate nucleus. J Neurosci. 33:12751–12763.